

PACS numbers: 87.19.uj; 87.63.L–; 87.64.kv; 87.85.Pq; 87.90.+y
DOI: 10.1070/QE2014v044n08ABEH015489

Optical diagnostics of vascular reactions triggered by weak allergens using laser speckle-contrast imaging technique

Yu.L. Kuznetsov, V.V. Kalchenko, N.G. Astaf'eva, I.V. Meglinski

Abstract. **The capability of using the laser speckle contrast imaging technique with a long exposure time for visualisation of primary acute skin vascular reactions caused by a topical application of a weak contact allergen is considered. The method is shown to provide efficient and accurate detection of irritant-induced primary acute vascular reactions of skin. The presented technique possesses a high potential in everyday diagnostic practice, preclinical studies, as well as in the prognosis of skin reactions to the interaction with potentially allergenic materials.**

Keywords: *laser speckle contrast imaging, exposure time, vasculature, skin, contact irritant, allergen.*

1. Introduction

Recently, due to the intense development of high technologies, including biophotonics, the methods of optical diagnosis of biological tissues are becoming increasingly widespread in various practical applications [1]. Among the problems of biomedical optics, the development and improvement of blood circulation diagnostic techniques is of particular importance. The major and most widely used optical methods of vascular bed imaging and blood flow monitoring include laser Doppler spectroscopy [2], laser Doppler flowmetry [3], confocal microscopy [4], optical coherence tomography (OCT) [5], Doppler OCT [6], colour Doppler OCT [7], correlation OCT [8], optical Doppler tomography [9], orthogonal polarisation of spectral images [10], dynamic light scattering [11], diffusing wave spectroscopy [12], laser speckle contrast (LSC) imaging [13], etc.

It was shown that the method of LSC imaging allows detection of even minor changes in microcirculatory blood flow, including the case of full cardiac arrest and occlusion of vessels [14]. At present, in combination with fluorescence intravital microscopy (FIM), this method is widely used for visualisation of vascular beds in skin blood vessels [15, 16], for studying the mechanisms that control microhemocirculation and rheological properties in microvessels surrounding a tumour and in the vascular bed [17] and for studying the blood and lymph microcirculation under the natural conditions [18, 19].

Within the framework of the present paper the possibility of using this method for direct visualisation and quantitative assessment of an acute and moderate skin reaction to the local action of an irritant is considered for the first time. The moderate skin reaction to the local action of a non-specific irritant or contact allergen is known to be most difficult for identification using the presently available diagnostic methods. In addition, the rapid growth of the number of patients with allergic diseases and other immune disorders attracts the attention of researchers to such a type of diagnostics, aimed at studying the causes and the methods of controlling immune mediated diseases [20]. Various xenobiotics, pollutants, professional sensitisers, medical preparations and many other factors can give rise to individual reactions in the organism, from pronounced immune suppression to high hypersensitivity.

To identify the danger of sensitisation or the risk of immune suppression, the preclinical methods of risk assessment in humans are being developed. The progress of prognostic screening tests aimed at revealing immunotoxic effects is closely related to preclinical studies with the model experiments using laboratory animals.

During a few decades the Guinea pigs were used in the studies of sensitising effect. Two types of induction exposure are used to form the hypersensitivity reaction in them, the adjuvant one with complete Freund's adjuvant (CFA) and the non-adjuvant one. The control allergen exposure can be implemented via the parenteral administration or application. The method requires large time expenditures, and for standardisation the observed changes in control and experimental animals are assessed in points using a descriptive scale. The optimised model is presently known as the Guinea Pig Maximisation Test (GPMT) [21].

Under certain circumstances other experimental animals can be used to get necessary information about sensitisation. Keeping in mind that 99% of genes in mice are similar to human ones, and taking into account the relatively low cost of mice, easy maintenance, high reproduction rate and small size, at present mice are most often used as laboratory animals [22]. In this connection the immune system of a mouse was studied in more detail than that of a Guinea pig. Moreover, with the progress of gene engineering technology now, in fact, it is possible to tailor-make genetically modified mice with a given degree of the disease of interest [22].

Yu.L. Kuznetsov, V.V. Kalchenko Department of Veterinary Resources, Weizmann Institute of Science, Rehovot, 76100, Israel
N.G. Astaf'eva V.I. Razumovsky Saratov State Medical University, Chair of Clinical Immunology and Allergology, ul. Bol'shaya Kazach'ya 112, 410012 Saratov, Russia;
I.V. Meglinski The Jack Dodd Centre for Quantum Technologies, Department of Physics, University of Otago, PO Box 56, Dunedin 9054, New Zealand; Research and Educational Institute of Optics and Biophotonics, N.G. Chernyshevsky Saratov State University, ul. Astrakhanskaya 83, 410012 Saratov, Russia;
e-mail: igor.meglinski@otago.ac.nz

Received 10 March 2014; revision received 11 May 2014
Kvantovaya Elektronika **44** (8) 713–718 (2014)
Translated by V.L. Derbov

With the aim of assessing the sensitisation potential in mice, the models were developed possessing a number of advantages, in particular, the possibility of objective assessment of the test final result, small duration and minimal procedure of animal treatment. This is, e.g., the local lymph node assay (LLNA) [23].

However, the mouse ear swelling test (MEST) [24] can be considered as the most promising presently. This test, developed in the early 1980s with the aim to make the assessment cheaper, shorter in time and more objective, became an alternative to the tests using the Guinea pig models.

Due to the implementation simplicity and relative rapidity of getting the results in many biological and preclinical studies, the MEST is accepted as the gold standard for noninvasive allergy test, which is widely used in everyday practice of testing new antiallergenic materials [24, 25]. In this test the substance under study (the potential allergen) is applied to the skin of mouse ear *in vivo*. The immune reaction of the organism to the substance is assessed by the degree of swelling, i.e., the thickness of the mouse ear in the location of substance application. The presence and the degree of skin swelling in the area of allergen application can be correlated with the allergen-induced local inflammation, irritation and hypersensitivity reaction. Unfortunately, the MEST is subjected to rather severe limitations, namely, the high variability when using small doses of allergens, the complexity of quantitative assessment of strong allergic reactions, etc. [25].

At the same time, using the MEST one can assess the activity not only of sensitisers and allergens, but also of any factors affecting microcirculation. Under the condition of standardisation and increased sensitivity, the field of MEST application can be essentially expanded. The test is used for the assessment of inflammation response in preimmune reactions, under the action of irritants or anti-inflammatory preparations [16–28]. The above reactions are associated with the local hemodiscirculatory processes (blood circulation failures), caused by the change of blood microcirculation, blood volume in the vascular bed, its rheological properties, or blood exit from the vessels [29–31]. As a consequence, the local velocity of blood flow in microvessels essentially varies in time. The situations are possible, when the microflows completely stop and then begin the motion in the opposite direction. In other words, the correlation time of fluctuating speckles varies, as for any random nonstationary process. That is why in order to visualise the primary acute vascular reaction of the skin to the local action of contact allergen we used the LSC imaging method with a long photodetector exposure time that has shown itself positively in the studies of complex nonstationary blood and lymph microcirculations *in vivo* [14, 18, 19].

2. Experimental

The used experimental setup for LSC imaging is a part of the multimodal optical diagnostic system, schematically presented in Fig. 1. The uniqueness of this diagnostic system consists in its capability of simultaneous exploitation of both imaging modes, LSC and FIM, under the natural conditions [15–19].

In the LSC imaging mode a laser diode LDM 808/3 LJ module (808 nm, 3 mW, Roither Lasertechnik, Austria) is used. The laser beam passes through the Thorlabs – Newton diffusor (USA) and illuminates the mouse ear. The speckles arising as a result of the reflection of diffusely scattered

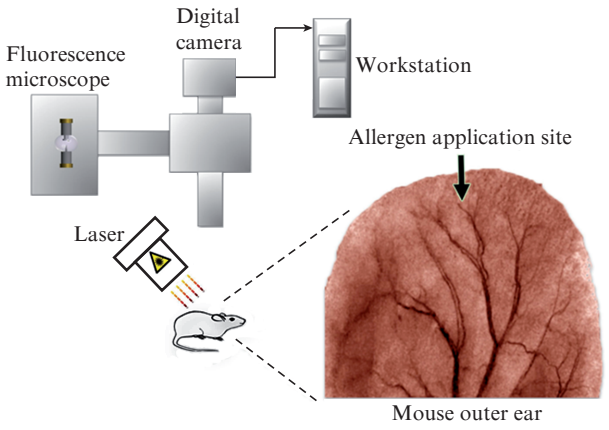

Figure 1. Schematic diagram of the experiment. The surface of mouse ear in the place of topical application of methyl salicylate is simultaneously illuminated with the mercury lamp of the fluorescent microscope and diffusely scattered laser light. The image detection in the LSC visualisation and/or FIM modes is implemented using the CCD camera, controlled by the personal computer.

light are recorded by means of a high-quality Pixelfly QE CCD camera (PCO, Germany) that allows the image capture with various exposure times within the range from 33 to 650 ms. The capture of a sequence of images (usually 300) and the camera control is implemented by means of the standard CamWare software (PCO, Germany). The processing and analysis of image sequence is implemented by using a special image processing software (eLSI) package for Fiji/Imagej [32].

The LSC visualisation method is based on the statistical analysis of intensity fluctuations of laser light, scattered by a biological tissue that contains such moving and light-scattering particles, as erythrocytes and lymphocytes. In the presence of blood and lymph flows and, therefore, the motion of scattering particles, the intensity of the scattered laser radiation fluctuates, forming nonstationary speckle patterns, varying in time. Quantitatively the motion of light-scattering particles is analysed using the degree of speckle contrast [33]:

$$K(T) = \sigma/\langle I\rangle, \tag{1}$$

where σ is the standard deviation from the mean intensity $\langle I\rangle$ at a given point of the speckle pattern. The degree of speckle contrast is a function of the detector exposure time T and the correlation time τ, inversely proportional to the mean velocity of the motion of scattering particles, and can be presented in the form [34]

$$K = \left\{\beta\rho^2 \frac{\exp(-2x) - 1 + 2x}{2x^2} + 4\beta\rho(1-\rho)\frac{\exp(-x) - 1 + x}{x^2} + v\right\}^{1/2}, \tag{2}$$

where $x = T/\tau$; the parameter β is defined by the ratio of the mean speckle size and the detector pixel size ($0 \leqslant \beta \leqslant 1$) and depends on the degree of polarisation and coherence of the probing light; ρ is the partial component of the dynamically scattered light (i.e., the light scattered by moving particles); and v is the spatial dispersion parameter that determines the experimental error, including the noise characteristics of the

detector (in our case, the CCD camera), the shot noise, the laser instability, etc. In the case of practical use of the LSC imaging technique for diagnostics and visualisation of blood flow, the parameters T and x are commonly not taken into account. It is *a priori* assumed that T exceeds τ ($T > \tau$). However, for a long detector exposure time ($T \gg \tau$) the sensitivity of the LSC imaging method increases even more [18, 19]. In the present work we used the LSC imaging method with a large detector exposure time ($T = 650$ ms).

In contrast to LSC, in the FIM mode the role of the light source is played by the short-arc mercury lamp, specially designed for fluorescence microscopes. The light, corrected by means of the optical filter with the transparency window from 460 to 490 nm, is reflected by the dichroic mirror and directed onto the same surface of the mouse ear, as in the method of LSC imaging. The detected fluorescence light passes through the band-pass optical filter with the transparency window 510–550 nm and arrives at the CCD camera (see Fig. 1). To obtain the fluorescent image of the blood vessels of the mouse outer ear in the FIM mode, 50 μL of dextran FITC (0.5 M, 10 mg mL^{-1}) is preliminarily injected intravenously. In the experiments we used female nude mice (CD-1 line from the Harlan Lab, Rehovot, Israel) with the age of 6–8 weeks. After the anaesthesia implemented by intraabdominal injection of the mixture of ketamine (Fort Dodge, USA) and xylazine (Kepro, the Netherlands), 10 mg kg^{-1} and 100 mg kg^{-1}, respectively, the animal was placed onto a warmed platform with a temperature controller. To avoid possible spontaneous movements of the animal during the experiment, the outer ear of the mouse was fixed with a double-faced scotch tape.

In spite of the principal difference between the used optical diagnostic methods, the spatial localisation of the detected signals in the LSC imaging and FIM method appears practically similar (Fig. 2). The distributions presented in Fig. 2 were obtained using the Monte Carlo (MC) method [35, 36], specially developed to assess the probability density (localisation) of the detected optical signal in the light-scattering medium under study for the presently available experimental setups with the possibility of distant calculations.

The spatial distribution of the detected signal is referred to as the sample volume. Generally, the sample volume depends on the optical properties of biotissues and will be different at different spatial positions of the source and the detector of optical radiation. It is shown that if the sample volume J is presented as a function of the depth r' in the medium, then it may be interpreted as a measure (conventionally, the probability density function) of the measurement sensitivity at the medium surface for the studied tissue volume, located at the depth r' [37]. Then the sample volume is expressed as

$$J(r_q, r_m, r') = \frac{\partial A(r_q, r_m)}{\partial \mu_a(r')}, \tag{3}$$

where $\partial\mu_a(r')$ is the increment of the absorption coefficient at the depth r', and $\partial A(r_q, r_m)$ is the increment of the decay amplitude at the point of the detector location with the coordinate r_m, provided that the source of light is placed at the point with the coordinate r_q. The decay amplitude is defined as

$$A(r_q, r_m) = -\ln\left(\frac{I(r_m)}{I_0(r_q)}\right). \tag{4}$$

Here $I_0(r_q)$ is the intensity of incident radiation at the point with the coordinate r_q, and $I(r_m)$ is the intensity of the detected reflected light at the point with the coordinate r_m. From Eqns (3) and (4) it follows that

$$J(r_q, r_m, r') = -\frac{1}{I(r_m)} \frac{\partial I(r_m)}{\partial \mu_a(r')}. \tag{5}$$

Thus, the sample volume is defined as the gradient of the specific radiation flux, recorded by the detector, with respect to the absorption coefficient of the small volume $\delta V(r')$ of the medium at the depth r'. The function $J(r')$ characterises the total spatial distribution of the detected optical radiation in the medium and is determined by the spatial distribution of effective optical paths. For a heterogeneous medium, consisting of a few homogeneous components with different optical

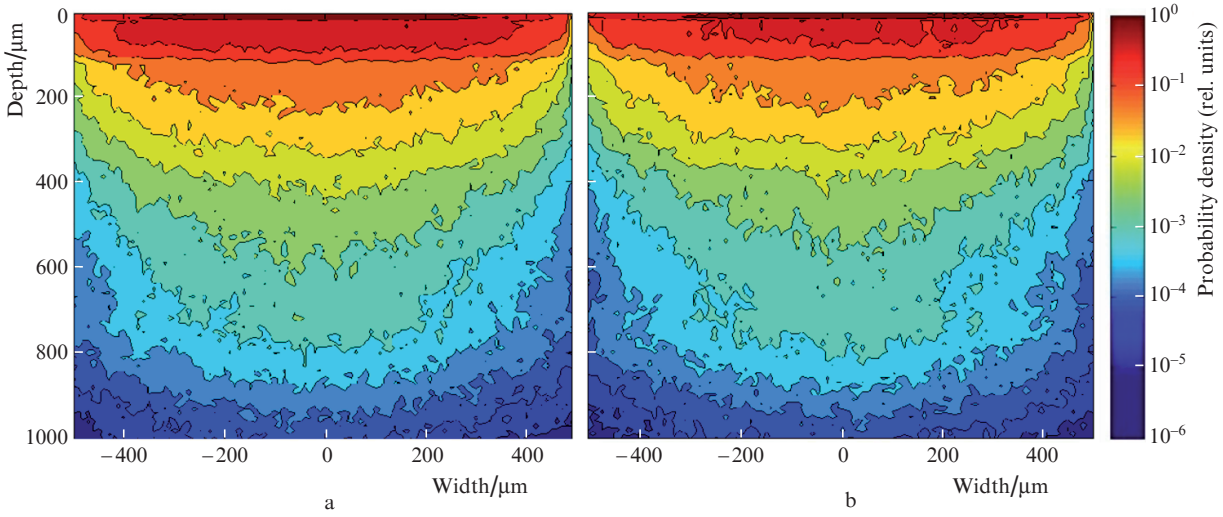

Figure 2. Localisation area spatial distributions of the detected signal in the near-surface tissues of the mouse ear skin, calculated using the Monte Carlo method [35, 36] for (a) LSC imaging and (b) FIM.

parameters, e.g., several optically homogeneous skin layers, the components of the sample volume have the form [38]

$$J_k(r') = -\frac{1}{I(r_m)}\frac{\partial I(r_m)}{\partial \mu_{ak}(r')}, \quad (6)$$

where μ_{ak} is the absorption coefficient of the kth medium layer. The sample volume $J_k(r')$ equals the mean free path length $\bar{L}(r)$ for the photons of the optical radiation, passing through the small volume $\delta V(r')$.

The numerical simulation using the Monte Carlo method is the most optimal method to assess the probability density of the distribution of effective optical paths (i.e., of the sample volume). The developed MC technique [35, 36] involves the concept of statistical weight (a measure of the given photon packet trajectory) that allows the description of the natural path of photon migration in the medium. This provides a possibility to introduce the concept of effective optical paths in the calculations. When the packet of photons arrives at the detector, its trajectories from the source to the detector are weighted using the final statistical weight W. Dividing the simulated medium into elementary volumes with the characteristic size $10 \times 10 \times 10$ μm and tracing the trajectory of each photon package from one volume to another, one can express the sample volume in the following way:

$$J(r') = -\frac{1}{I(r_m)}\frac{\partial I(r_m)}{\partial \mu_{ak}(r')} = \frac{\sum_{i=1}^{N_{ph}} L_i(r')\, W_{di}(r_m)}{l_0 \sum_{i=1}^{N_{ph}} W_{di}(r_m)}. \quad (7)$$

Here W_{di} is the final weight of the ith detected photon packet; N_{ph} is the total number of the detected photon packets; $L_i(r')$ is the path length traversed by the ith photon packet in the elementary volume with the centre at the depth r'; and l_0 is the size of this volume.

Thus, the sample volume (see Fig. 2) is a 2D rectangular mesh $J(x, z)$ obtained from the 3D distribution $J(r')$, where x is the horizontal axis (width) and z is the depth. To determine the path length in an elementary volume, the algorithm based on the Cohen–Sutherland line clipping method was implemented. The technique of $J(r')$ calculation is presented and discussed in more detail in Ref. [38].

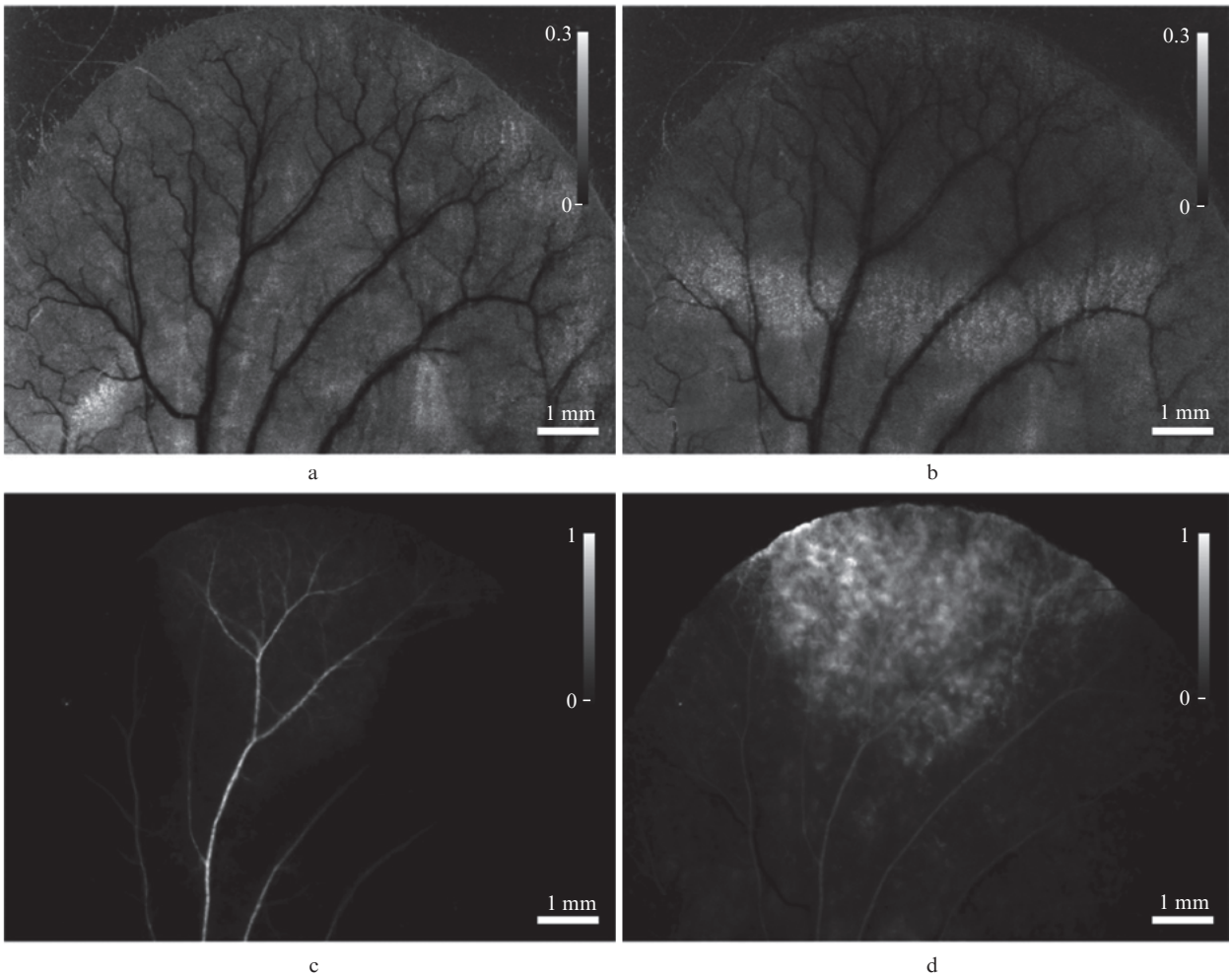

Figure 3. Monochrome images of mouse ear *in vivo* obtained by means of the LSC imaging method with a long detector exposure time (650 ms) under normal conditions (a) and in 30 min after the local application of methyl salicylate (b) [small values of speckle contrast (intensity scale, dark colour) correspond to the increased blood flow], as well as the images, obtained using the FIM method with intravenous injection of dextran FITC before (c) and after (d) the local application of methyl salicylate.

3. Results and discussion

Positive reaction of the LLNA test was observed as a result of applying the solution of methyl salicylate to the mouse ear skin during 30 min under natural conditions (Fig. 3). The methyl salicylate was topically applied to the skin of the mouse outer ear, and the final vascular reaction was identified as distinctly observable tissue edema. The exit of the fluorescent contrast substance beyond the limits of the vascular bed and its accumulation in the surrounding tissues of the outer ear is clearly seen in the place of the contact irritant action. In the present work the major attention was focused on the possibility of quantitative assessment of the acute vascular reaction to the local action of methyl salicylate on the mouse ear skin without preliminary sensitisation.

It was found that the acute vascular reaction to the action of allergen/irritant at early stages manifests itself in the increased vascular permeability, which gives rise to massive efflux of plasma from capillaries into the adjacent interstitial spaces, vasodilatation and edema [39]. This essentially decreases the blood flow in small vessels, such as venules, arterioles, and capillaries. It is shown that the slowing of erythrocyte motion at early stages of this process may be efficiently observed using the LSC imaging method [14, 15]. Actually, the edema reaction is not the only process that occurs as a result of the increased blood vessel permeability. In most cases the inflammation process, including allergic reaction, causes a local lymphatic dysfunction, which is characterised by the slowing of lymph flow, lymphedema, etc. [39, 40]. In Refs [18, 19] it was shown that the LSC imaging method using a large detector exposure time is sensitive to local variations of the lymph flow intensity and can be used to visualise the latter. The results presented in Fig. 3 are also obtained by means of the LSC imaging method using a long exposure time ($T = 650$ ms) and demonstrate good agreement with the results of the studies mentioned above.

Allowing for the fact that the vessel permeability monitoring may be a key subject in the assessment of the acute vascular reaction, as well as in the verification of results obtained by means of the LSC imaging method, we repeated the experiment with the use of FIM imaging method. The increased permeability of vessels was clearly seen in 30 s after the injection of dextran FITC. It looks like a light area (Fig. 3d), located in the vicinity of blood vessels. Hence, the results of visualising the mouse ear skin response to the action of irritant (potential allergen or sensitising agent), obtained by means of the FIM method, confirm the results of LSC imaging.

4. Conclusions

Thus we have shown that the LSC imaging method with a long detector exposure time ($T \approx 650$ ms) can be used for noninvasive observation of the acute vascular reaction of skin to the action of methyl salicylate. The FIM imaging mode within the framework of the present experiment is used mainly as a verifying method. The obtained results demonstrate essential potential of the developed technique for application in everyday practice of preclinical investigations. The method is also promising for everyday diagnostic practice of assessing contact hypersensitivity, prognosis of skin reactions to potential allergens, sensitisers and to the interaction with a wider spectrum of xenobiotics, environment pollutants, various chemicals, medical preparations and other materials that can be used for application. The method will help in the prognosis of transdermal transport of medical preparations and the evaluating the efficiency of transdermal pharmaceutical forms.

The relative simplicity and the low cost of practical implementation of the LSC imaging method in everyday clinical practice are also worth noting. The authors express their confidence that the adaptation of the described technique to everyday practice of allergic tests, performed on human skin, will allow using reduced amount of allergen at the expense of high sensitivity of the LSC imaging method.

Acknowledgements. This work was supported by the Lewis Family Trust (VK) and Weizmann Institute of Science (Israel).

The authors also express their gratitude to the Otago University, New Zealand (PBRF Research Output Publishing Grant).

References

1. Tuchin V.V. *Lazery i volokonnaya optika v biomeditsinskikh issledovaniyakh* (Lasers and Fibre Optics in Biomedical Studies) (Moscow: Fizmatlit, 2010).
2. Priezzhev A.V., Romanovskii Yu.M. *Kvantovaya Elektron*., **5** (10), 2237 (1978). [*Sov. J. Quantum Electron*., **8** (10), 1260 (1978)].
3. Krupatkn A.I., Sidorov V.V. *Lazernaya dopplerovskaya fluorimetriya mikrostirkulyatsii krovi* (Laser Doppler Fluorimetry of Blood Microcirculation) (Moscow: Meditsina, 2005).
4. Rajadhyaksha M. et al. *J. Invest. Dermatol*., **104**, 946 (1995).
5. Bonesi M. et al. *Laser Phys*., **20**, 891 (2010).
6. Bonesi M. et al. *J. Innovative Opt. Health Sci*., **2**, 431 (2009).
7. Izatt J.A. et al. *Opt. Lett*., **22**, 1439 (1997).
8. Doronin A., Meglinski I. *Laser Photonics Rev.*, **7**, 797 (2013).
9. Chen Z. et al. *IEEE J. Sel. Top. Quantum Electron*., **5**, 1134 (1999).
10. Messmer K. *Orthogonal Polarization Spectral Imaging, Progress in Applied Microcirculation* (Basel: Karger, 2000).
11. Fine I. et al. *Laser Phys*., **22**, 469 (2012).
12. Meglinski I., Tuchin V.V., in *Handbook of Coherent-Domain Optical Methods. Biomedical Diagnostics, Environmental Monitoring and Material Science.* Ed. by V.V. Tuchin (New York: Springer, 2012) Vol. 1, Ch.3, pp 149–166.
13. Boas D.A., Dunn A.K. *J. Biomed. Opt*., **15**, 011109 (2010).
14. Meglinski I.V., Kal'chenko V.V., Kuznetsov Yu.L., Kuznik B.I., Tuchin V.V. *Dokl. Ross. Akad. Nauk*, **451**, 393 (2013) [*Dokl. Phys*., **58** (8), 323 (2013)].
15. Kalchenko V. et al. *Laser Phys. Lett*., **7**, 603 (2010).
16. Kuznetsov Yu.L., Kal'chenko V.V., Meglinski I.V. *Kvantovaya Elektron*., **41** (4), 308 (2011) [*Quantum Electron*., **41** (4), 308 (2011)].
17. Kalchenko V. et al. *J. Biophotonics*, **4**, 645 (2011).
18. Kalchenko V. et al. *J. Biomed. Opt*., **17**, 050502 (2012).
19. Kal'chenko V.V., Kuznetsov Yu.L., Meglinski I.V. *Kvantovaya Elektron*., **43** (1), 679 (2013) [*Quantum Electron*., **43** (1), 679 (2013)].
20. Adkinson N.F. Jr. *Middleton's Allergy: Principles and Practice* (Philadelphia, PA: Mosby Elsevier, 2008).
21. Basketter D.A. et al. *Food Chem. Toxicol*., **30**, 65 (1992).
22. Rosenthal N., Brown S. *Nat. Cell Biol*., **9**, 993 (2007).
23. Montelius J. et al. *Acta Derm. Venereol*., **78**, 433 (1998).
24. Gad S.C. et al. *Toxicol. Appl. Pharmacol*., **84**, 93 (1986).
25. Garrigue J.L. et al. *Contact Dermatitis*, **30**, 231 (1994).
26. Anderson S.E. et al. *Toxicol Sci*., **127**, 371 (2012).
27. Gerbeix C. et al. *Toxicol Sci*., **134**, 39 (2013).
28. Moallem S.A. et al. *Iran. J. Basic Med. Sci*., **16**, 1238 (2013).
29. Mchedlashvili G.I. *Mikrotsirkulyatsiya krovi: Obschie zakonomernosti regulirovaniya i narushenii* (Blood Microcirculation: General Laws of Regulation and Abnormalities) (Leningrad: Nauka, 1989).

30. Kupriyanov V.V., Karaganov Ya.L., Kozlov V.I. *Mikrotsirkulyatornoye ruslo* (Microcirculatory Bed) (Moscow: Meditsina, 1975).
31. Chernukh A.M., Aleksandrov P.N., Alekseev O.V. *Mikrotsirkulyatsii* (Microcirculations) (Moscow: Meditsina, 1984).
32. Schindelin J. et al. *Nat. Methods*, **9**, 676 (2012).
33. Briers J.D. et al. *J. Biomed. Opt*., **4**, 164 (1999).
34. Parthasarathy A.B. et al. *Opt. Express*, **16**, 1975 (2008).
35. Doronin A., Meglinski I. *Biomed. Opt. Express*, **2**, 2461 (2011).
36. Doronin A., Meglinski I. *J. Biomed. Opt*., **17**, 090504 (2012).
37. Arridge S. *Appl. Opt*., **34**, 7395 (1995).
38. Meglinski I.V., Bashkatov A.N., Genina E.A., Churmakov D. Yu., Tuchin V.V. *Kvantovaya Elektron*., **32** (10), 875 (2002) [*Quantum Electron*., **32** (10), 875 (2002)].
39. Emanuel M.B. *Clin. Exp. Allergy*, **29**, 1 (1999).
40. Miteva D.O. et al. *Circ Res*., **106**, 920 (2010).